Downloaded from https://academic.oup.com/gji/article/224/3/2001/6029122 by Univ of Calif, San Diego (Ser Rec, Acq Dept Library) user on 15 January 2021

Geophysical Journal International



doi: 10.1093/gji/ggaa559

Geophys. J. Int. (2021) 224, 2001–2015 Advance Access publication 2020 December 9 GJI Geomagnetism, rock magnetism and palaeomagnetism

Detrital remanent magnetization of single-crystal silicates with magnetic inclusions: constraints from deposition experiments

Liao Chang, ^{1,2} Hoabin Hong, ¹ Fan Bai, ¹ Shishun Wang, ¹ Zhaowen Pei, ¹ Greig A. Paterson ⁶, ³ David Heslop, ⁴ Andrew P. Roberts, ⁴ Baochun Huang, ¹ Lisa Tauxe ⁶⁵ and Adrian R. Muxworthy ⁶⁶

Accepted 2020 November 17. Received 2020 November 15; in original form 2020 May 26

SUMMARY

Quasi-linear field-dependence of remanence provides the foundation for sedimentary relative palaeointensity studies that have been widely used to understand past geomagnetic field behaviour and to date sedimentary sequences. Flocculation models are often called upon to explain this field dependence and the lower palaeomagnetic recording efficiency of sediments. Several recent studies have demonstrated that magnetic-mineral inclusions embedded within larger non-magnetic host silicates are abundant in sedimentary records, and that they can potentially provide another simple explanation for the quasi-linear field dependence. In order to understand how magnetic inclusion-rich detrital particles acquire sedimentary remanence, we carried out depositional remanent magnetization (DRM) experiments on controlled magnetic inclusion-bearing silicate particles (10-50 µm in size) prepared from gabbro and mid-ocean ridge basalt samples. Deposition experiments confirm that the studied large silicate host particles with magnetic mineral inclusions can acquire a DRM with accurate recording of declination. We observe a silicate size-dependent inclination shallowing, whereby larger silicate grains exhibit less inclination shallowing. The studied sized silicate samples do not have distinct populations of spherical or platy particles, so the observed size-dependence inclination shallowing could be explained by a 'rolling ball' model whereby larger silicate particles rotate less after depositional settling. We also observe non-linear field-dependent DRM acquisition in Earth-like magnetic fields with DRM behaviour depending strongly on silicate particle size, which could be explained by variable magnetic moments and silicate sizes. Our results provide direct evidence for a potentially widespread mechanism that could contribute to the observed variable recording efficiency and inclination shallowing of sedimentary remanences.

Key words: Magnetic properties; Magnetic mineralogy and petrology; Palaeointensity; Palaeomagnetism; Rock and mineral magnetism.

1 INTRODUCTION

Sedimentary palaeomagnetism provides long and continuous records of past variations of geomagnetic field direction and intensity, which are used widely in the Earth sciences for dating sedimentary sequences, and for understanding rapid geomagnetic changes and associated deep-Earth dynamo processes (e.g. Tauxe 1993; Valet et al. 2005; Roberts et al. 2013; Tauxe & Yamazaki

2015). In many sedimentary settings, magnetic polarity is accurately recorded and is used in geochronology through correlation of polarity sequences to the geomagnetic reversal timescale (e.g. Gradstein *et al.* 2012). Sedimentary records also provide a globally coherent pattern of what has been interpreted as variations in the geomagnetic dipole strength (e.g. Valet *et al.* 2005; Channell *et al.* 2009; Ziegler *et al.* 2011), although a sound theoretical basis for understanding signal recording is lacking (e.g. Roberts *et al.* 2013).

¹Laboratory of Orogenic Belts and Crustal Evolution, School of Earth and Space Sciences, Peking University, 100871 Beijing, China. E-mail: liao.chang@pku.edu.cn

²Laboratory for Marine Geology, Qingdao National Laboratory for Marine Science and Technology, 266071 Qingdao, China

³Department of Earth, Ocean and Ecological Sciences, University of Liverpool, Liverpool, UK

⁴Research School of Earth Sciences, Australian National University, Canberra, ACT 2601, Australia

⁵Scripps Institution of Oceanography, University of California San Diego, La Jolla, CA 92093-0220, USA

⁶Department of Earth Science and Engineering, Imperial College London, London, UK

Acquisition of sedimentary remanence is a complex process that is explained using the depositional remanent magnetization (DRM) and post-depositional remanent magnetization (PDRM) concepts, where a range of physical, chemical, and biological processes can affect remanence acquisition (Tauxe 1993; Tauxe & Yamazaki 2015). Sediment remanence acquisition involves several progressive processes: (1) settling through a water column (e.g. Nagata 1961; Heslop et al. 2006; Tauxe et al. 2006; Heslop 2007), (2) rotating, rolling, and slipping of particles due to mechanical interactions when encountering the substrate (e.g. King 1955; Griffiths et al. 1960; Jezek et al. 2012; Bilardello 2013; Bilardello et al. 2013) and (3) PDRM associated with bioturbation, dewatering, compaction, diagenesis, etc. (e.g. Kent 1973; Verosub 1977; Roberts et al. 2013; Egli & Zhao 2015; Zhao et al. 2016). Particle interactions in the water column and interactions of particles with the substrate lead to inclination shallowing (Bilardello et al. 2013). The strength of sedimentary palaeomagnetic signals is also sensitive to variations in the constituent magnetic mineral types and their mixtures, including detritus from weathered source rocks, biogenic and authigenic minerals, as well as associated variations in magnetic mineral concentration and grain size (Roberts et al. 2013). Despite the challenge of understanding sedimentary remanence acquisition, globally synchronous palaeomagnetic signals (e.g. Valet et al. 2005; Channell et al. 2009; Ziegler et al. 2011) and the laboratory-observed strong quasi-linear field dependence of remanence (e.g. Johnson et al. 1948; Tauxe 1993; Paterson et al. 2013; Valet et al. 2017) provide a foundation for high-resolution sedimentary relative palaeointensity (RPI)

Our knowledge of sedimentary remanence acquisition has improved significantly due to recent theoretical and empirical understanding of individual processes that contribute to sedimentary remanences (e.g. Tauxe and Kent 1984; Tauxe et al. 2006; Heslop 2007; Mitra & Tauxe 2009; Roberts et al. 2013; Egli & Zhao 2015). Simple theoretical models (Nagata 1961) predict that magnetic particles deposited through a viscous medium such as water should align fully with an external magnetic field essentially instantaneously. Such models contrast with the laboratory-observed field-dependence of DRM acquisition that indicates a much lower recording efficiency (e.g. Johnson et al. 1948; Tauxe 1993; Tauxe et al. 2006). Sediment flocculation models have been proposed to explain this low recording efficiency, where magnetic particles adhere to the surface of, or are embedded within, larger particles, known as flocs, to produce lower net magnetic moments that can reduce palaeomagnetic recording efficiency (Shcherbakov & Shcherbakova 1983; Van Vreumingen 1993a, b). More recent numerical flocculation models (e.g. Tauxe et al. 2006; Mitra & Tauxe 2009) can explain quantitatively the depositional data and also predict a nonlinear DRM dependence for smaller flocs (i.e. several micrometres). Shcherbakov & Sycheva (2010) pointed out that many parameters are needed to describe sedimentary remanence acquisition and highlighted limitations of flocculation models; by tuning model parameters, depositing flocs can align fully with an external field given sufficient settling times (e.g. in oceanic settings). Sediment resuspension events, which have variable occurrence and frequency in aquatic environments, complicate DRM acquisition because of their shorter settling times.

Recently, a further mechanism was proposed that can also contribute to lower sedimentary palaeomagnetic recording efficiency (Chang *et al.* 2016a; Chen *et al.* 2017; Hong *et al.* 2019), which is associated with sedimentary silicate host particles with magnetic mineral inclusions embedded within them (Hounslow & Maher 1996; Hounslow & Morton 2004; Maher *et al.* 2009; Hatfield

et al. 2013; Chang et al. 2016a, b). Bilardello (2013) and Bilardello et al. (2013) conducted the first deposition experiments using magnetic inclusion-bearing synthetic glass particles of controlled shapes to investigate DRM acquisition of plates and spheres, including spherical glass beads and glass flakes containing iron and magnetite impurities. Compared to a single magnetic particle model, the inclusion model has a reduced effective magnetic moment for two reasons: (1) host silicates are non-magnetic and will lower the volume-normalized magnetization of bulk particles and (2) the thermoremanent magnetization (TRM) carried by an assemblage of magnetic inclusion particles will have a net magnetic moment of only a few per cent compared to the magnetic moment of individual particles (Chang et al. 2016a) because of the weak alignment that results in lower TRMs and other natural remanences compared to perfectly aligned individual grains (Butler 1992). This smaller magnetic moment will reduce the recording efficiency because settling of larger host particles will be dominated by gravitational and hydrodynamic forces rather than by geomagnetic torques (e.g. Heslop 2007).

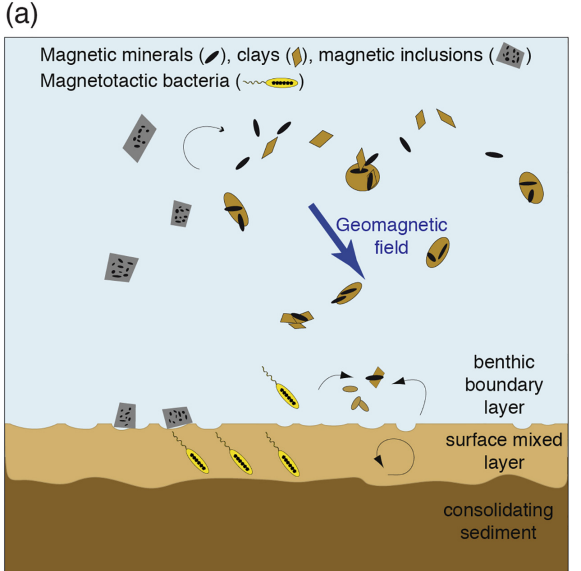
In order to investigate the DRM behaviour of magnetic mineral inclusions in silicates and their contributions to sedimentary remanence (Fig. 1a), we carried out laboratory deposition experiments, using well-characterized silicate host particles with magnetic inclusions. Our experiments document the DRM behaviour of magnetic mineral inclusions as a function of host silicate particle size and external magnetic field.

2 SAMPLES AND METHODS

Gabbro and mid-ocean ridge basalt (MORB) samples were used as two igneous source rocks for the DRM experiments. These samples are known to contain abundant magnetic mineral inclusions embedded in silicates. The gabbro sample is from the Modipe Gabbro from the Botswana/South Africa border (Evans *et al.* 1968; Muxworthy & Evans 2013; Muxworthy *et al.* 2013). The MORB sample is from the ultra-slow spreading Southwest Indian Ridge (Tao *et al.* 2014; Wang *et al.* 2020).

To prepare samples for DRM experiments, fresh rock pieces were crushed into fine-grained powders and were then subjected to magnetic separation using rare-earth magnets. The magnetically extracted powders were bathed in hydrochloric acid (HCl; 3 mol 1⁻¹ concentration) to dissolve unprotected Fe/Ti oxide grains. The solution turned yellow after 1 d and samples were then washed with de-ionized water three times. HCl was added to the sample again; this procedure was repeated three times until a nearly clear solution was observed, which indicates that unprotected Fe/Ti oxides were dissolved. Fe/Ti oxide inclusions embedded within silicates remained intact because they are protected by silicate host grains that are not reactive to HCl. After chemical treatment, samples were washed in de-ionized water and were dried in an oven at 25 °C for 2 d. Finally, we used different mesh sizes (10, 15, 20, 30 and 50 μ m) to sieve silicate particles into specific size ranges (10-15, 15-20, 20–30 and 30–50 μ m). Samples are named 'MORB 10–15 μ m', 'gabbro 30–50 μ m', etc.

Sieved powdered samples (i.e. sister samples of those used for DRM experiments) were subjected to scanning electron microscope (SEM) observations and to magnetic measurements. Powder samples were mounted in epoxy resin and were polished for SEM observations. SEM observations were carried out with a FEI Quanta 650 field emission SEM at 15 keV at the School of Earth and Space Sciences (SESS), Peking University (PKU), China. Hysteresis,



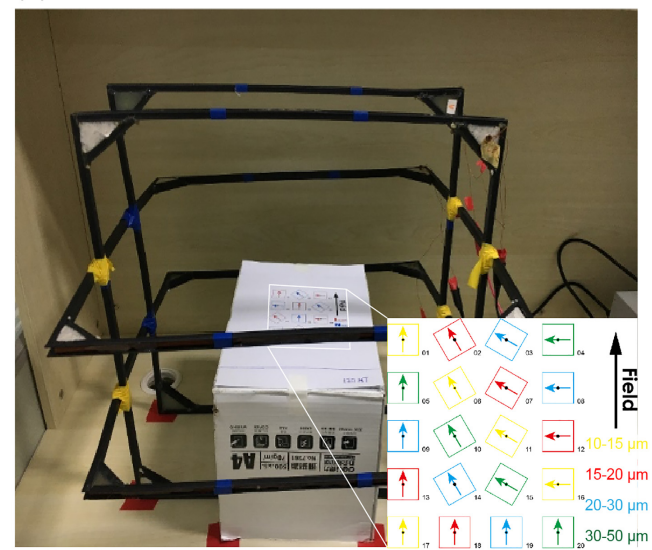


Figure 1. (a) Schematic illustration of the sediment magnetization processes involving various magnetic particle types in Earth's magnetic field (modified from Tauxe *et al.* 2006). Magnetic mineral inclusions embedded in non-magnetic minerals are included. (b) Experimental set up. Inset in (b) indicates position and orientation (numbers and small arrows) of cubes used for deposition experiments within the 2-axis Helmholtz coils. The field direction (thick black arrow) was fixed during deposition experiments. The colours represent arrangements for experiments with different grain sizes.

(b)

isothermal remanent magnetization (IRM) acquisition and backfield demagnetization, and first-order reversal curve (FORC; Roberts et al. 2000) measurements were made on powder samples with a LakeShore vibrating sample magnetometer (VSM; model 8600) at the Institute of Geomechanics, Chinese Academy of Geological Sciences, Beijing. Hysteresis loops were measured between -1and +1 T with a 5 mT field step and 250-300 ms averaging time. Hysteresis parameters, including the saturation magnetization (M_s), the saturation remanent magnetization (M_{rs}) , the coercive force (B_c) and the coercivity of remanence (B_{cr}) were extracted from loops and backfield curves. FORC measurements were made with a 1 T maximum applied field, 2.7 mT field increment and 350 ms averaging time. FORC diagrams were produced with the FORCinel 3.06 software (Harrison and Feinberg 2008) using the VARIFORC algorithm (Egli 2013). Magnetic susceptibility was measured with an AGICO MFK1-FA Kappabridge system. An anhysteretic remanent magnetization (ARM) was imparted on packed powder samples with a 100 mT peak alternating field (AF) and a 50 μ T direct current (DC) bias field using an ASC D2000T demagnetizer. An IRM at 1 T was imparted with an ASC IM-10-30 pulse magnetizer. IRM and ARM intensities were measured with a 2-G Enterprises superconducting rock magnetometer. Susceptibility, IRM and ARM measurements were made at the SESS, PKU.

Helmholtz coils were used to control the magnetic field environment for the DRM experiments. For each set of deposition experiments, five sister samples from each sized sample were arranged within the centre of the 2-axis Helmholtz coils as sketched in Fig. 1(b). First, $\sim\!0.05$ g of sized material was mixed with deionized water and was then transferred into standard 2 \times 2 \times 2 cm palaeomagnetic cubes and sealed. After shaking the cubes to randomize particle orientation, the cubes were placed inside the Helmholtz coils. The sediment settled in laboratory-controlled fields for over one hour after which a thin layer of a few millimetres at the bottom of the cube was seen. The resulting DRM was measured by carefully inserting the cube into a 2-G Enterprises

superconducting rock magnetometer (model 755; noise level 3 × 10^{-12} Am²) housed in a magnetically shielded room at the SESS, PKU. The discrete sample cryogenic magnetometer at PKU has a 4.2 cm access diameter. The thin sample shape should not have a significant effect on magnetic moment measurements. In addition, this experimental setting has a deposition length of less than 2 cm. Shaking the sample cubes increases particle-particle and particlewall interactions, which has been found to lead to increased inclination shallowing (Jezek et al. 2012; Bilardello et al. 2013). Depositional environments that form such thin layer samples are different from many natural sedimentary settings (although similar to instantaneous records in high sedimentation rate environments) so palaeomagnetic data for these thin samples are not always directly comparable to those of natural sediment samples. Nevertheless, our DRM data sets (e.g. remanence intensity and inclination) should be comparable among our series of laboratory deposition experiments to reveal silicate-size dependent DRM acquisition. Two main sets of DRM experiments were undertaken at PKU by systematically changing the field intensity and inclination. For one set, the field was set with an inclination of 45° , with declinations of 0° , 30° , 60° and 90°, and variable field intensities from 0 to 160 μ T in 10 μ T steps. For another set, the intensity was fixed at 45 μ T with declinations of 0°, 30°, 60° and 90°, and with inclination varying from 0° to 90° in 10° steps. In any set field intensity and direction, DRM results for five sister samples with the same grain size were recorded (inset in Fig. 1b).

3 RESULTS

3.1 Mineralogical and magnetic characterizations of samples

SEM observations indicate that the prepared silicate particles have relatively homogenous sizes with magnetic inclusions (Fig. 2). No obvious isolated, unprotected iron/titanium oxide grains are evident.

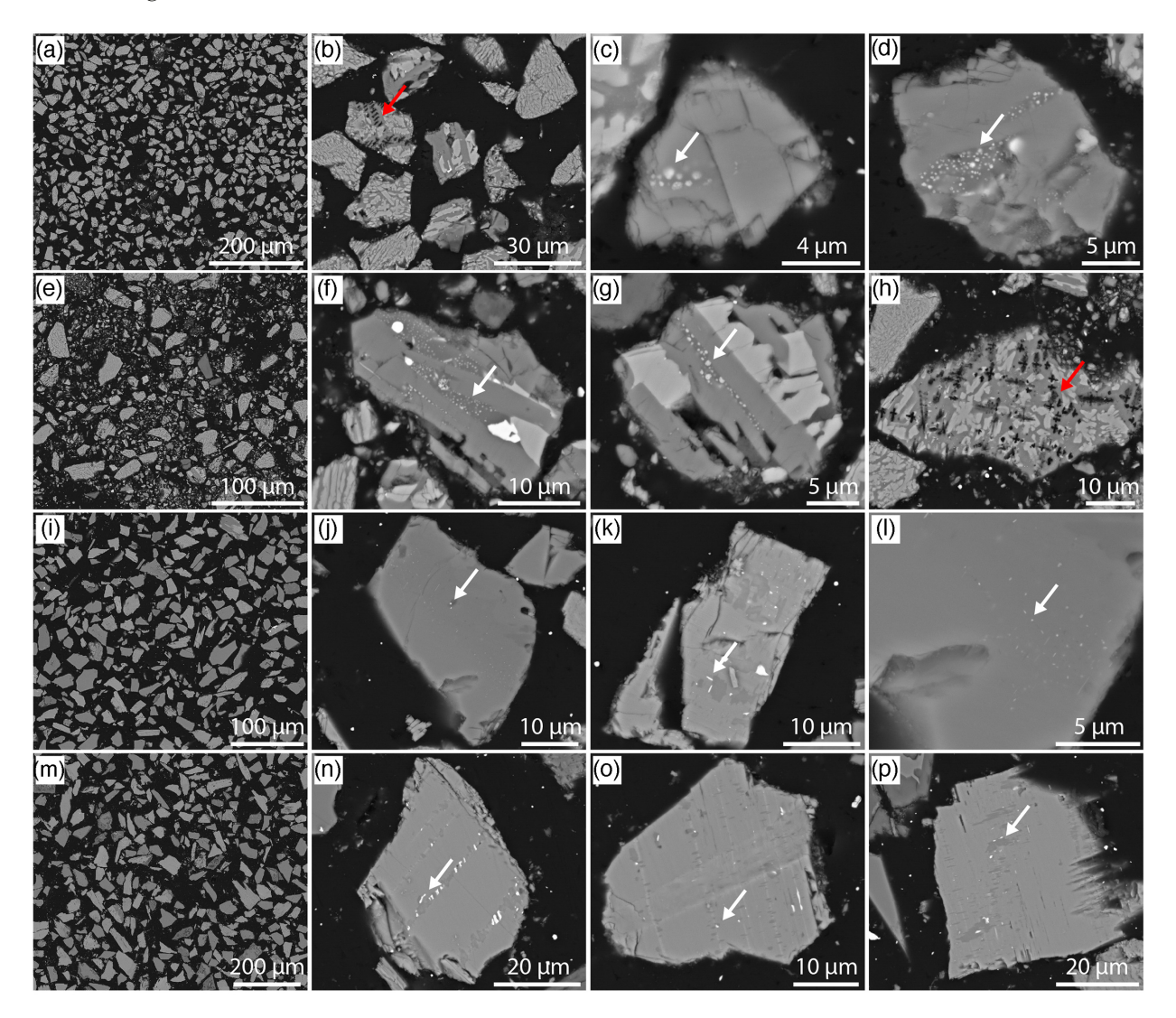


Figure 2. Back-scattered SEM images of typical sized silicate samples used for depositional experiments: (a–d) 'MORB 10–15 μ m', (e–h) 'MORB 20–30 μ m', (i–l) 'gabbro 10–15 μ m' and (m–p) 'gabbro 20–30 μ m'. Overview images are shown on the left. Other images are of single silicate grains containing magnetic mineral inclusions. White arrows in (c–g, j–p) indicate fine-grained (titano)magnetite inclusions. Red arrows in (b, h) point to relict dendritic structures (black appearance), where the original titanomagnetite dendrites were dissolved during chemical treatment of samples.

SEM images of the sized gabbro and MORB samples indicate the common presence of fine-grained (titano)magnetite particles that appear as isolated or clustered grains embedded in silicates (Fig. 2; white arrows). Silicate grains in MORB samples (Figs 2a-h) apparently contain more abundant and closely spaced magnetic mineral inclusions, compared to the gabbro samples (Figs 2i-p). Sieved silicates in MORB samples consist of a mixture of pyroxene and plagioclase. Gabbro samples contain needle-like magnetic mineral inclusions, as indicated by microscopic studies on samples from the same locality (Evans et al. 1968). The sieved silicates in gabbro samples consist of pyroxene. In addition, we observe the common presence of relict dendritic structures (black in SEM images; Figs 2b, h, red arrows). This indicates that original titanomagnetite dendrites on silicate surfaces were dissolved by HCl during chemical leaching, while magnetic inclusions within silicate interiors remained intact. This feature further confirms the effectiveness of our chemical treatment to produce pure magnetic mineral inclusion bearing samples.

The sizes of silicate grains are distinct among different samples (Figs 2a, e, i and m). We counted and measured many polished silicate grains in SEM images for three samples (with 634–1211 grains counted; Table 1): 'MORB 10–15 μ m', 'gabbro 10–15 μ m' and 'gabbro 20–30 μ m' (Fig. 3). Statistical properties of particle length and shape distributions are given in Table 1. The mean particle length for each sample is near the sieved size range (Figs 3a, c and e; Table 1). Some samples have a relatively large grain length dispersion (Fig. 3e). Particle lengths smaller than the mesh size occur because grain dimension measurements were made on polished sections, where some grains were only exposed partially after polishing (Fig. 2). The presence of particles with lengths larger than the mesh size probably results from their elongation, so that they passed through the sieve due to their small narrow dimension.

Table 1. Silicate particle size and elongation statistics for selected sized silicate samples measured from SEM images.

Samples	MORB 10–15 μm	Gabbro 10–15 μm	Gabbro 20–30 μm
Particle number	1119	1211	634
Mean length (μ m)	17.3	18.6	34.2
median length (μ m)	16.5	17.5	33.1
IQR of length (μm)	9.3	10.2	22.8
Mean elongation	1.72	1.81	1.92
Median elongation	1.60	1.66	1.69
IQR of elongation	0.70	0.77	0.88

Note: IQR, Interquartile range.

SEM observations of our sized silicate samples (Fig. 2) indicate that grain shape and elongation for the three studied samples is similar (Figs 3b, d and f; Table 1). Our observations also do not reveal distinct populations of more spherical or platy particles, although the larger sample 'gabbro $20{-}30~\mu{\rm m}$ ' has a slightly larger grain elongation (length/width ratio) compared to sample 'gabbro $10{-}15~\mu{\rm m}$ ' (Fig. 3f; Table 1). Nevertheless, particle sizes are distinct among different samples with subtle grain elongation differences.

Hysteresis loops, IRM acquisition curves, and backfield demagnetization curves for whole rock samples and sized silicate samples are presented in Fig. 4; hysteresis parameters are given in Table 2. There is a small decreasing trend in M_s values with increasing grain size among the sized MORB samples (Table 2). Other rock magnetic properties are similar among the sized MORB silicate samples, but are distinct from the bulk MORB sample (Figs 4a and b). This is consistent with SEM observations, which indicate that significant amounts of unprotected dendritic titanomagnetite grains were removed chemically from the bulk sample during production of the sized silicates. Magnetic properties for the gabbro whole rock sample and sized silicate samples are similar (Figs 4c and d), although $M_{\rm rs}/M_{\rm s}$ ratios are slightly lower than reported by Muxworthy & Evans (2013) for optically handpicked pyroxene crystals from the same gabbro outcrop. Muxworthy & Evans (2013) showed that after separating the handpicked samples into four subsamples based on pyroxene opaqueness, the M_{rs}/M_s ratio increases. The lower M_{rs}/M_s values in this study represent an average hysteresis response for the pyroxene crystals. M_s values among the sized gabbro samples are similar and do not have a notable grain size dependent trend (Table 2).

A FORC diagram for the bulk MORB sample contains concentric contours with large vertical spread (Fig. 5a), which indicates the dominance of magnetostatically interacting stable single domain (SD) and vortex state grains (Roberts et al. 2014, 2017; Lascu et al. 2018). Sized MORB samples have contrasting FORC signatures compared to the bulk MORB sample, but similar FORC diagrams are obtained for different sized samples with elongated concentric distributions along the horizontal axis and small/moderate vertical spreading (Figs 5b-e), which correspond to weakly/moderately interacting SD assemblages (Roberts et al. 2000, 2014). A faint 'zero to negative' ridge oriented at $\sim 135^{\circ}$ for the MORB samples (vertical arrows; Figs 5a-e) represents vortex-state grains (Lascu et al. 2018). A FORC diagram for the bulk gabbro sample contains a predominantly teardrop-like concentric distribution with a long high-field tail (Fig. 5f), which indicates the presence of interacting and weakly interacting SD and vortex state grains (Roberts et al. 2014, 2017; Lascu et al. 2018). The negative FORC distribution values along the negative B_u axis (horizontal arrows; Figs 5f-j) are consistent with the presence of uniaxial SD grains (Muxworthy et al. 2004; Newell 2005; Egli *et al.* 2010). The bulk and sized gabbro samples (Figs 5f–j) have similar FORC diagrams: in agreement with FORC diagrams reported by Muxworthy and Evans (2013) (pyroxene crystals) and Muxworthy *et al.* (2013) (whole rock). Sized gabbro samples in this study have slightly greater contributions from the low-coercivity component with larger vertical spread (Figs 5g–j), likely due to vortex state grains (Roberts *et al.* 2017). FORC diagrams are similar among the sized gabbro samples (Figs 5g–j).

In summary, SEM observations and magnetic measurements confirm that the sized gabbro and MORB samples have relatively well-controlled silicate sizes and compositions. Each sized sample set has similar mineralogical and magnetic properties. All prepared samples contain pure magnetic mineral inclusions hosted within silicates (i.e. isolated magnetic mineral grains were chemically removed). The main difference between sized samples is the average silicate size.

3.2 Depositional experiments

Results of DRM acquisition experiments conducted in various set field intensities and directions are presented in Figs 6–8 and in Table S1–S3. DRM directional data indicate that declinations are recorded accurately (Figs 6a and c; black lines). This result demonstrates that magnetic inclusion-bearing samples acquire a DRM. In contrast to accurate declination recording, inclinations are shallow, as has been observed in many DRM experiments (e.g. King 1955; Griffiths et al. 1960; Tauxe & Kent 1984; Zhao & Roberts 2010; Bilardello 2013; Bilardello et al. 2013; Zhao et al. 2016; Molinek & Bilardello 2018). The DRM data have a clear inclination shallowing trend as a function of silicate size: (1) sized gabbro samples have a higher degree of flattening (i.e. lower f values of \sim 0.2–0.4) compared to the MORB samples (f values of \sim 0.3–0.5) and (2) f values for gabbro and MORB samples are size-dependent, where larger silicates have a smaller degree of inclination shallowing (Figs 6b and d).

Field dependent deposition experiments indicate a monotonic DRM intensity increase with field intensity for both sample sets (Fig. 7), with some scatter, for example DRM data for MORB samples at 50 and 110 μ T (Figs 7d–f). This scatter is likely due to experimental errors. Despite these small deviations, all normalized DRM intensities indicate a clear non-linear relationship between remanence and applied field over the 0–100 μ T range (Fig. 7).

We observe a DRM dependence on silicate host particle size. For both gabbro and MORB samples, mass-normalized DRM (Figs 7a and d) has higher values for smaller particles (10–15 μ m). Sized MORB samples have a slightly decreasing M_s with increasing grain size (Table 2), which may contribute partially to the observed size-dependent mass-normalized DRM data (Fig. 7d). Sized gabbro samples do not have a grain size dependent M_s (Table 2), yet these samples have a grain size dependent mass-normalized DRM (Fig. 7a). Such grain size dependent DRM may be explained in terms of inclination shallowing increasing the length of the resultant vector for settling fields <45°, whereas deposition in fields >45° resulted in shortening of the resultant vector (Jezek & Gilder 2006), although experimental conditions in this study are different to those modeled by Jezek & Gilder (2006).

Other normalized DRM ratios have a more complex size dependent behaviour, which might result from slight magnetic property variations among different sized samples. We also plot DRM as a function of inclination (Fig. 8), which indicates a strong inclination dependence for constant field intensity during DRM acquisition: normalized DRM values are highest at zero inclination (horizontal)

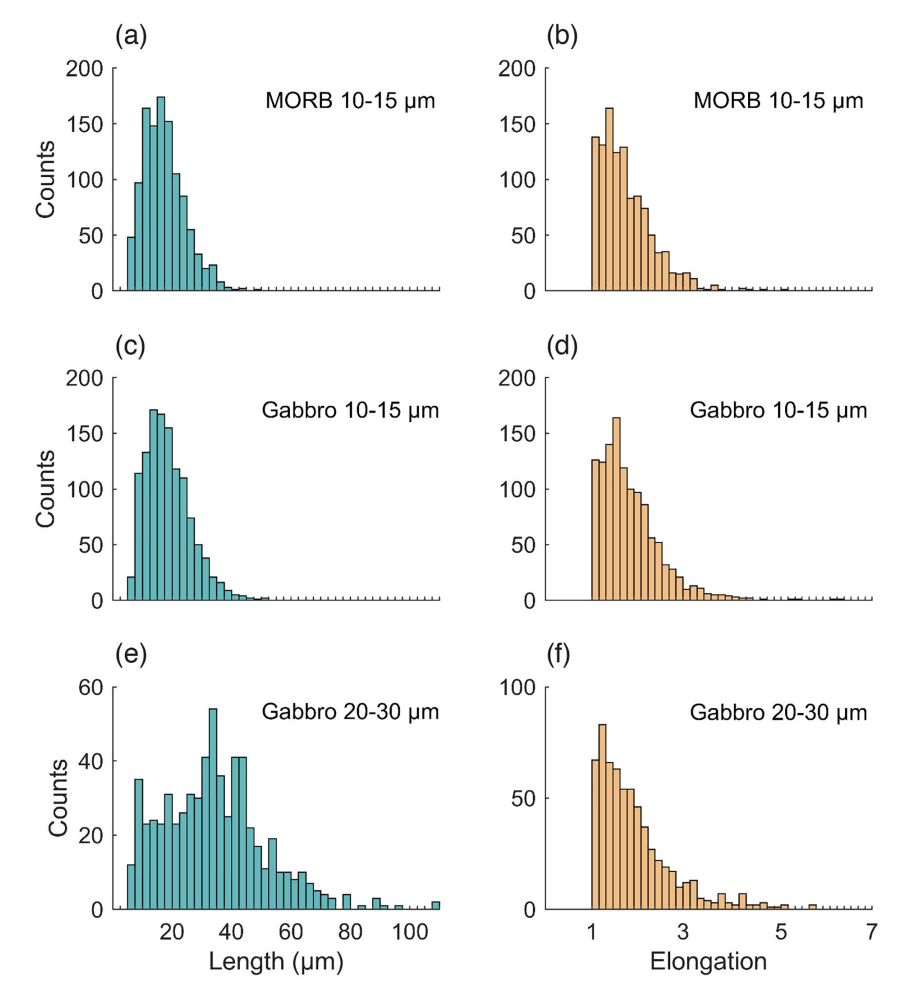


Figure 3. (a, c, e) Measured grain length and (b, d, f) grain shape distributions of three typical sized silicate samples from SEM images, where 1119, 1211 and 634 grains were counted for samples 'MORB 10–15 μ m', 'gabbro 10–15 μ m' and 'gabbro 20–30 μ m', respectively.

and lowest when the field is vertical, in agreement with previous observations (Tauxe & Kent 1984; Molinek & Bilardello 2018). While our DRM results for samples with different size fractions have larger intensity spread in horizontal versus vertical fields, these differences become more constant after normalization (Figs 8b, c, e and f). This demonstrates the validity of normalization to account for different magnetic behaviour in samples for RPI determination (e.g. Levi & Banerjee 1976; Tauxe & Yamazaki 2015).

4 DISCUSSION

4.1 Magnetic inclusions as an explanation for low remanence acquisition efficiency

Nagata (1961) presented a calculation for magnetic particle deposition in a magnetic field *B* (that drives particle rotation by a magnetic torque) through a viscous medium (that opposes particle rotation by viscous drag) and obtained:

$$\tan\frac{\alpha}{2} = \tan\frac{\alpha_0}{2} \exp\left(-\frac{mBt}{\lambda}\right),\tag{1}$$

where α is the angle between the magnetic moment m of the grain and the external field B, α_0 is the initial angle and λ is the viscosity

coefficient. λ represents the viscous drag and is a complex function of the fluid viscosity η (i.e. fresh or salt water) and geometry of depositing particles, such as particle size (Tauxe *et al.* 2006) and shape (Jezek and Gilder 2006; Heslop 2007).

Considering a simple case of spherical particles($\lambda = 8\pi r^3 \eta$; where r is the particle radius) and Eq. (1), the characteristic time τ (where the angle α reduces to α_0/e) for aligning the magnetic moment m of a spherical particle with an external magnetic field B is given by:

$$\tau = \frac{8\pi r^3 \eta}{mB},\tag{2}$$

Using values for the viscosity of water ($\sim 10^{-3}$ kg m⁻¹ s⁻¹), an Earth-like magnetic field ($20-100~\mu T$), and the volume magnetization of a single spherical grain for typical ferrimagnetic minerals, such as magnetite, eq. (2) gives a short τ (i.e. < 1 s) such that magnetic grains align with the external field almost instantly. Assuming no other forces, this suggests that a DRM for an ensemble of magnetic mineral grains should have an efficient remanence acquisition with intensity close to saturation that is effectively independent of the external field strength (Tauxe *et al.* 2006). This prediction contrasts with experimental observations (e.g. Johnson *et al.* 1948; Tauxe *et al.* 2006; Mitra & Tauxe 2009) that sedimentary DRMs are

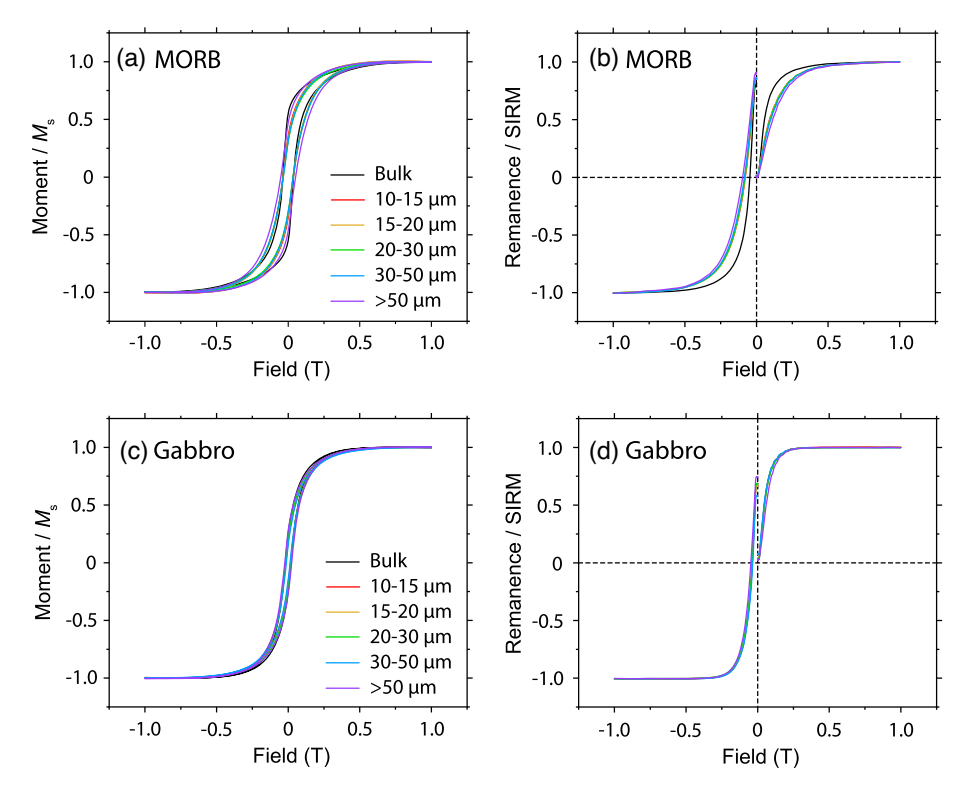


Figure 4. (a, c) Hysteresis loops and (b, d) IRM acquisition and backfield demagnetization curves for the depositing sized silicate samples (data in colours) and whole rock samples (data in black). Magnetization data are normalized to saturation values. Hysteresis parameters are given in Table 2.

Table 2. Hysteresis parameters for the studied bulk igneous rock and sized samples.

Table 2. Hydretesis parameters for the station come ignorus from and sized samples.							
Samples	$B_{\rm c}~({\rm mT})$	B _{cr} (mT)	$M_{\rm s}~({\rm Am^2~kg^{-1}})$	$M_{\rm rs}/M_{\rm s}$	$B_{\rm cr}/B_{\rm c}$		
MORB bulk	36.7	46.1	1.073E-01	0.55	1.26		
MORB 10–15 μ m	35.8	78.2	3.028E-02	0.35	2.18		
MORB 15–20 μm	33.8	79.1	2.546E-02	0.33	2.34		
MORB 20–30 μ m	33.2	80.9	2.629E-02	0.31	2.44		
MORB 30–50 μm	33.6	84.8	2.185E-02	0.31	2.52		
MORB 50–100 μm	51.4	97.1	8.602E-03	0.47	1.89		
Gabbro bulk	18.9	37.5	3.301E-02	0.25	1.98		
Gabbro 10–15 μm	16.1	38.0	5.068E-02	0.18	2.36		
Gabbro 15–20 μm	16.5	37.7	4.356E-02	0.20	2.28		
Gabbro 20–30 μm	17.6	38.8	4.230E-02	0.21	2.20		
Gabbro 30–50 μm	12.6	34.4	5.578E-02	0.15	2.73		
Gabbro 50–100 μ m	23.4	47.0	3.063E-02	0.27	2.01		

often less efficient than suggested by eq. (2) and are field dependent. Sediment flocculation models have been proposed to explain the DRM inefficiency (Shcherbakov & Shcherbakova 1983; van Vreumingen 1993a, b), where aggregation of magnetic particles with non-magnetic particles (e.g. clays) and magnetic moment cancellation within composite flocs (Tauxe $et\ al.\ 2006$; Mitra & Tauxe 2009), greatly reduces the net magnetization M, thereby increasing τ .

Deposition of silicate host particles with embedded magnetic mineral inclusions should have a similar effect as flocculation because the silicate host is not magnetic and because of magnetic moment cancellation within inclusions (Chang *et al.* 2016a) that greatly reduces their alignment by geomagnetic torques (i.e. increasing τ). In order to assess the ability of magnetic inclusion-bearing silicate grains to align with the field, we calculate τ values

as a function of magnetic moment m (or volume magnetization M) for a spherical magnetic silicate particle with radius r using eq. (2) (Fig. 9). Expected τ values for two cases are considered using: (1) reported remanence values for hand-picked single crystal silicates (Tarduno et al. 2001, 2006; Tarduno & Cottrell 2005), and (2) typical remanence values of bulk igneous rocks. For case (1), saturation IRM (SIRM) values for strongly magnetic, hand-picked single silicate crystals (upper shaded region in Fig. 9) lie well above the $\tau=1$ s line (i.e. they correspond to small τ values where magnetic grains align rapidly with the field). TRMs for hand-picked single silicate crystals lie near the $\tau=1$ s line. For case (2), we consider silicate grains with typical natural remanent magnetization (NRM) values for igneous rock samples that fall in the 0.1–10 A m⁻¹ range (cf. ter Maat et al. 2019), where the studied MORB samples have values of \sim 10 A m⁻¹ (Wang et al. 2020), and the gabbro samples

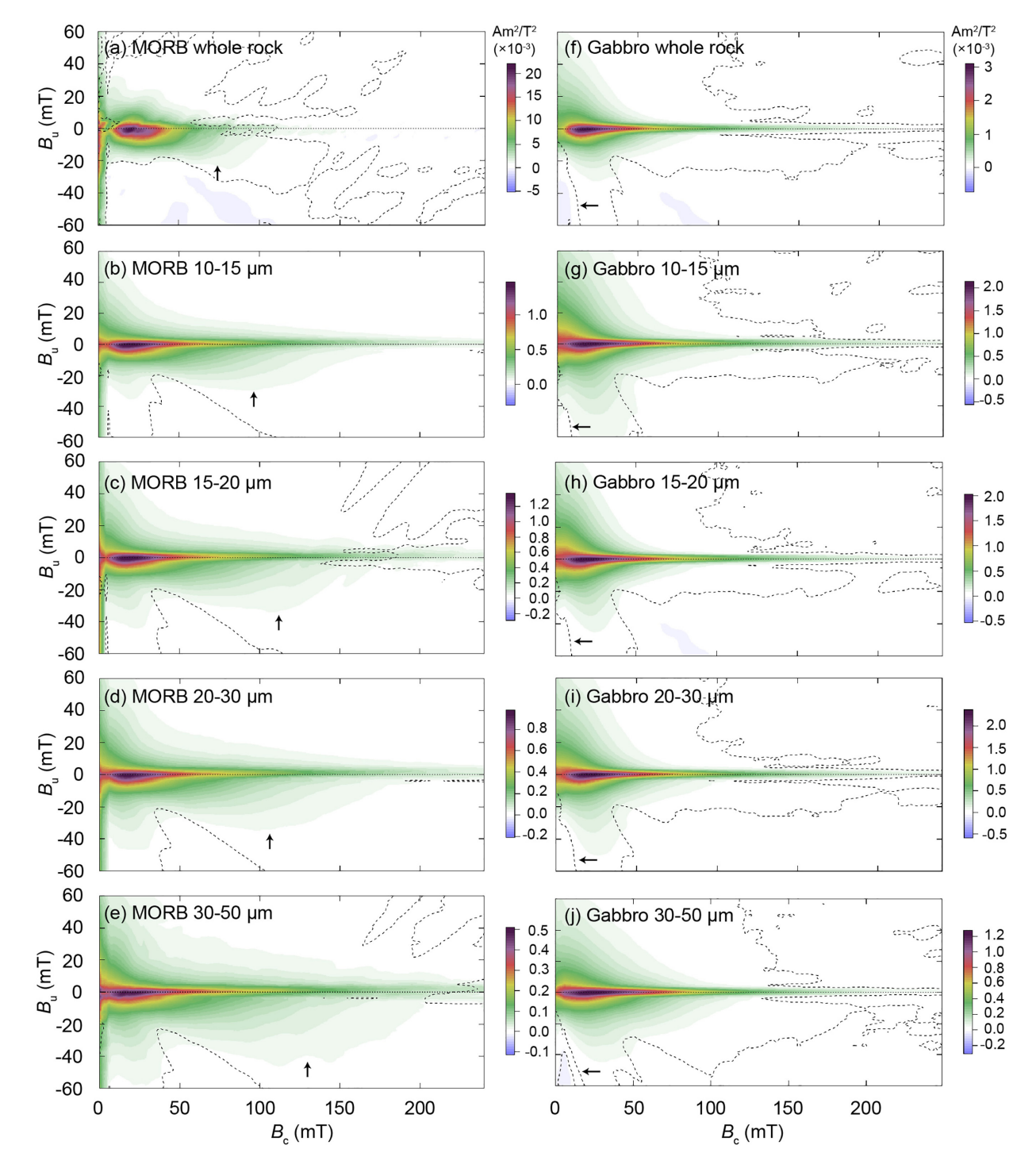


Figure 5. FORC diagrams for the bulk rock (top) and size fraction samples used for depositional experiments. Dashed lines indicate the 0.05 significance level (Heslop and Roberts 2012). VARIFORC (Egli 2013) smoothing parameters ($S_{c0} = 4$, $S_{b0} = 3$, $S_{c1} = S_{b1} = 7$) were used for all FORC diagrams.

have values of $\sim 1-6$ A m⁻¹. Using magnetization values of 0.1–10 A m⁻¹, we obtain τ values between 12 s and 20 min (dashed lines in Fig. 9). Silicate particle elongation will increase viscous drag during settling (i.e. Jezek & Gilder 2006; Heslop 2007) and

 τ . Our magnetic extraction of silicate host particles likely magnetized particles close to their SIRM values, which would have erased their original TRM. Single silicate crystal SIRMs are much larger (\sim 25 times greater) than TRMs. Magnetic moment cancellation

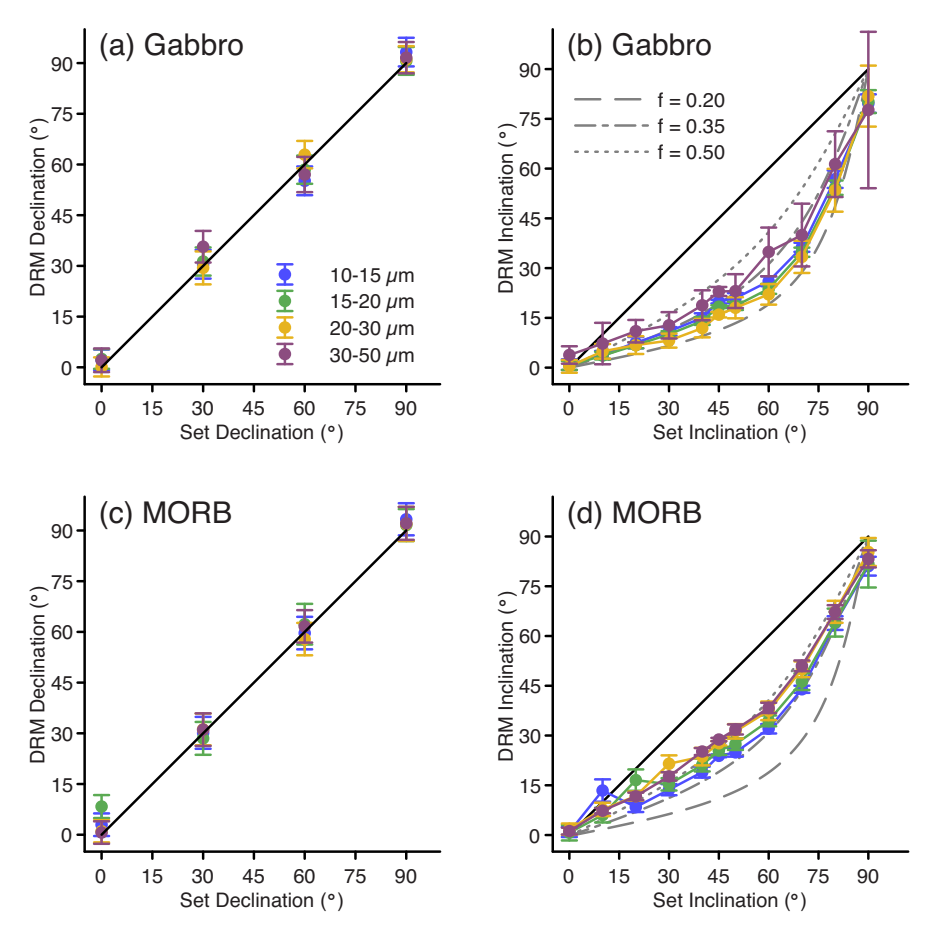


Figure 6. Recorded (a, c) DRM declination and (b, d) inclination with respect to set direction values for sized (a, b) gabbro and (c, d) MORB samples. DRM experimental settings: declinations of 0° , 30° , 60° , 90° , inclinations of 0° , 10° , ..., 90° , and a fixed magnetic field of 45 μ T. Black lines in (a-c) are the one-to-one ratio lines. Dashed lines in (b, d) are typical curves for different values of the empirical flattening factor f (King 1955). Error bars represent one standard deviation (Table S1). Colours represent different grain size fractions.

within inclusions in our DRM experiments is, thus, likely much suppressed. This could explain the much larger experimental DRM ratios (e.g. DRM/ARM and DRM/SIRM; Figs 7b, c, e and f) compared to palaeomagnetic records (e.g. Chen et al. 2017). Regardless, we expect that deposition of silicate single crystals with TRMs may produce a more linear field dependence of DRM intensity because their lower magnetic moments (Fig. 9) will fall into the more linear lower-field DRM region (Fig. 7). Remanence acquisition is also inevitably affected by particle motion when encountering the substrate. Several experimental and numerical studies have demonstrated magnetic moment dispersion for both platy and spherical particles due to particle rolling and slipping, which can further reduce the remanence when particles touch the substrate (Jezek et al. 2012; Bilardello 2013; Bilardello et al. 2013). For example, Jezek et al. (2012) demonstrated numerically that slipping, rather than rolling, in smaller particles maintains the moment orientation, while larger particles are affected by rolling to reduce the DRM.

In summary, magnetic and morphological properties of natural silicate grains are variable, which will produce variable τ values during deposition that range from seconds to minutes, with τ for some magnetically weak silicates approaching an hour (Fig. 9). Silicate particles with different sizes and shapes also have different

settling times. Such variable relaxation and deposition times are likely the cause of gradual silicate alignment with external fields during deposition to produce a quasi-linear field dependence. Our DRM experiments demonstrate that host silicate particles with sizes up to $50~\mu m$ record geomagnetic field information with two caveats: (1) the recorded DRM inclination is shallow and (2) RPI has a non-linear field dependence. These observations directly confirm experimental and numerical studies (Jezek *et al.* 2012; Bilardello 2013; Bilardello *et al.* 2013; Chang *et al.* 2016a; Chen *et al.* 2017; Hong *et al.* 2019) and demonstrate that deposition of host particles with magnetic inclusions provides a further mechanism for field-dependent DRM acquisition.

4.2 Sedimentary remanence acquisition of magnetic inclusion-bearing particles

Tauxe et al. (2006) obtained an empirical expression for the deposition velocity of spherical grains as a function of grain radius:

$$\tan\frac{\alpha}{2} = \tan\frac{\alpha_0}{2} \exp\left(-\frac{mBl}{8.8\pi \eta r^{3.78}}\right),\tag{3}$$

where l is the deposition length, eq. (3) and considering λ for a general case suggests that the DRM intensity of silicates with

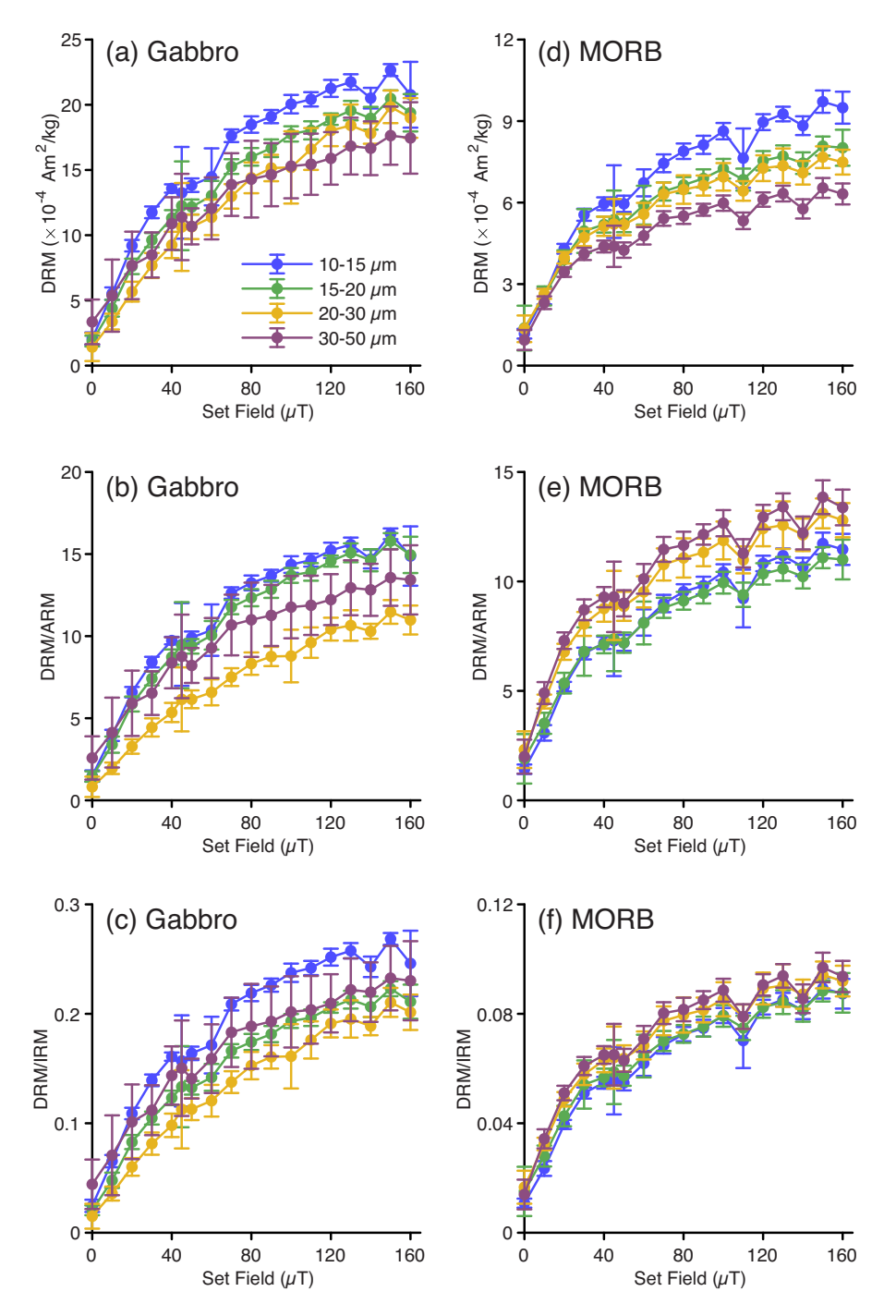


Figure 7. Recorded 'RPI' with different normalizers as a function of the set magnetic field for sized (a–c) gabbro and (d-f) MORB samples. DRM experimental settings: magnetic fields of 0, 10, ..., 160 μ T; declination of 0°, 30°, 60°, 90°, and a fixed inclination of 45°. Error bars represent one standard deviation (Table S2). Colours represent different grain size fractions.

magnetic inclusions is controlled by: (1) silicate host grain size, (2) the net magnetic moment of silicates, (3) the external field *B* and (4) water column height (deposition length). Our deposition experiments demonstrate clearly effects (1)–(3). For example, magnetic moment distributions in silicates for gabbro and MORB samples could explain their different DRM behaviour. The effect of silicate size on DRM behaviour is also demonstrated (Figs 6–8). The

exact distributions of magnetic moment m and size r for the silicate grains, which produce variable τ during deposition (Fig. 9), should partially control the shape of the field-dependence of DRM intensity. Silicate host grain sizes are well defined and the magnetic properties of magnetic mineral inclusion assemblages can also be characterized in detail, which makes them suitable model materials to understand sediment magnetization acquisition.

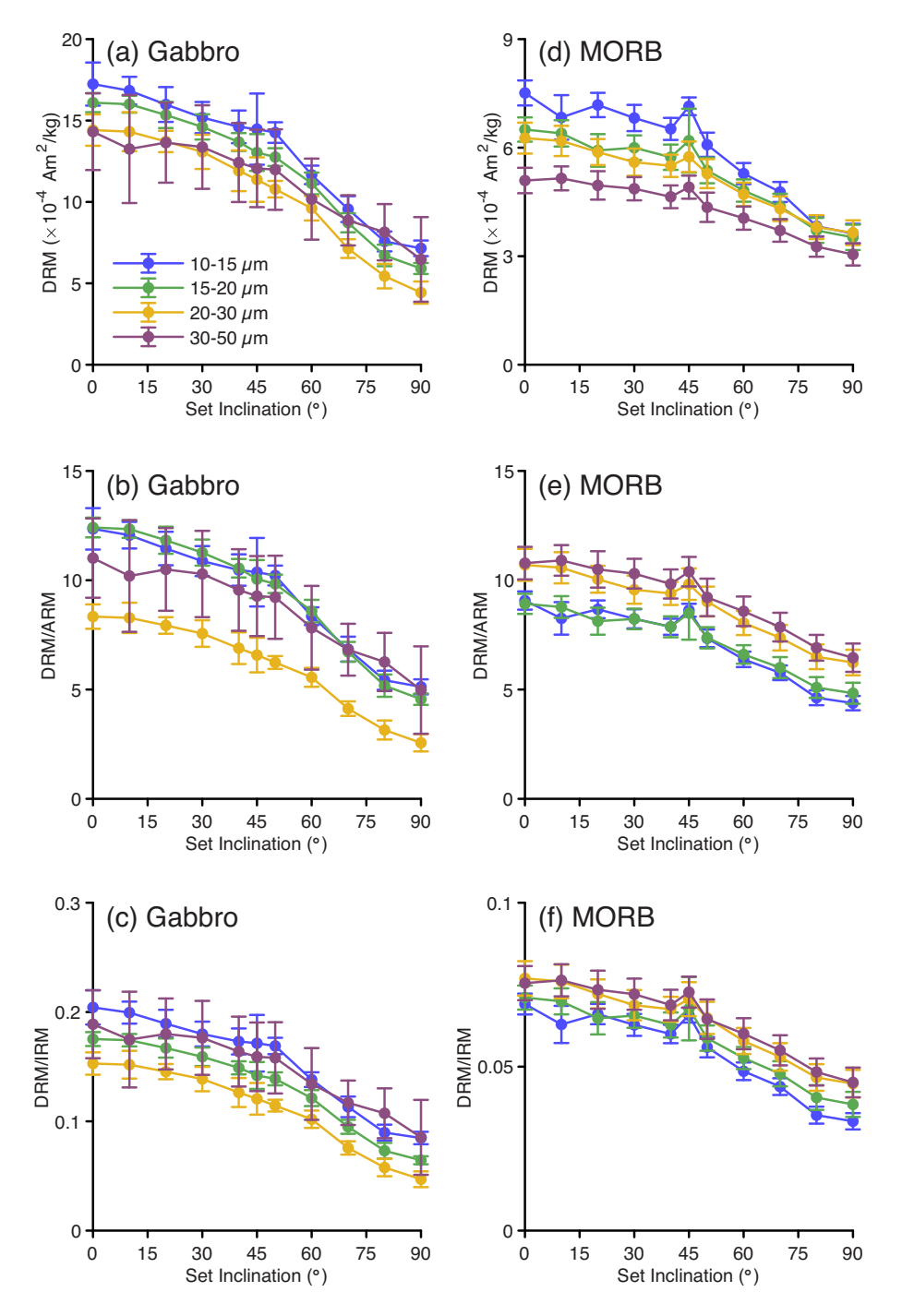


Figure 8. Recorded 'RPI' with different normalizers as a function of the set inclination for the sized (a–d) gabbro and (e–h) MORB samples. DRM experimental setting: declinations of 0° , 30° , 60° , 90° , inclinations of 0° , 10° , ..., 90° , and a fixed $45-\mu T$ field. Error bars represent one standard deviation (Table S3). Colours represent different size fractions.

We calculated deposition times considering deposition lengths and Stokes's Law. Our experiments were conducted within 2-cm boxes, so the maximum settling distance of particles is <2 cm with a 0–2 cm range of settling distances. The fact that a clear DRM signal is recorded indicates that a significant fraction of depositing particles achieved magnetic alignment within a 2-cm water column. The settling velocity ν of spherical particles is given by Stokes's

Law:

$$v(r) = \frac{2}{9} \frac{(\rho - \rho_{\rm w}) gr^2}{\eta},\tag{4}$$

where ρ and $\rho_{\rm w}$ are densities of the depositing particle and water, respectively, r is the particle radius and g is the gravitational acceleration. Considering a maximum 2-cm deposition length for the 1, 10,

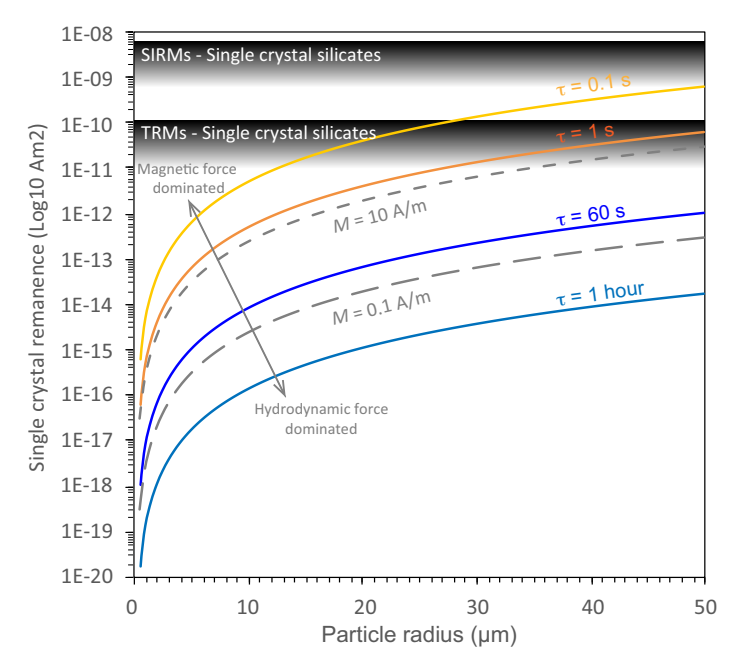


Figure 9. Remanence plotted as a function of particle radius of single crystal silicates for different τ values using eq. (2). Silicate crystals below a particular τ line cannot be aligned with the field during this characteristic time τ . Upper left-hand and lower right-hand regions (indicated by an arrow) are for grains dominated by magnetic and hydrodynamic forces, respectively. The following parameters were used: $B = 50 \mu T$, $\eta = 10^{-3} \text{ kg m}^{-1} \text{ s}^{-1}$. Typical SIRM and TRM values reported for single crystal silicates (Tarduno *et al.* 2001; Tarduno and Cottrell 2005; Tarduno *et al.* 2006) are indicated (0.5–5 × 10⁻⁹ Am² and 1–10 × 10⁻¹¹ Am² intervals for SIRMs and TRMs, respectively). These values are for hand-picked and magnetically stronger single crystal silicates. In natural depositional environments, detrital silicates can have much smaller sizes and magnetic moments than those of hand-picked silicate single crystals used in absolute palaeointensity studies (Tarduno *et al.* 2006). Dashed lines were calculated following eq. (2) considering various volume magnetization M values from igneous rock NRMs.

20, 30 and 50 μ m depositing particles, we obtain deposition times of ~77 min, ~46 s and ~11 s, ~5 s and ~2 s, respectively. These estimated settling times are comparable to the calculated characteristic alignment time τ during deposition (Fig. 9). It is therefore possible that in our DRM experiments, some large silicate particles may not have had sufficient time to align with the external magnetic field before settling, which would produce a slightly weaker remanence for larger size fractions (Figs 8a and d).

Brownian motion could also affect sedimentary remanence acquisition and produce a field dependent DRM intensity ($M_{\rm DRM}$) by randomizing magnetic moments in fluids by thermal agitation (Collinson, 1965). The Brownian motion model describes the DRM intensity by the Langevin expression, which is similar to thermal fluctuation effects on paramagnetic magnetization (Collinson, 1965):

$$M_{\rm DRM} = mn \left(\cot \alpha - 1/\alpha\right),\tag{5}$$

where $\alpha = mB/\kappa T$, m is the magnetic moment of the grain, n is the number of particles per unit volume, κ is Boltzmann's constant $(1.38 \times 10^{-23} \, \text{J K}^{-1})$ and T is temperature. In eq. (5), $\alpha < 1$ defines the region with a high Brownian motion influence. For isolated magnetite grains, such as magnetite $(M = 4.8 \times 10^5 \, \text{A m}^{-1})$, $\alpha < 1$ (using $B = 50 \, \mu \text{T}$; $T = 300 \, \text{K}$) predicts a small upper size of $\sim 69 \, \text{nm}$ for spherical grains. Silicates hosting magnetic mineral inclusions have much lower magnetization compared to isolated magnetic mineral grains, so it is expected that the maximum silicate size for which Brownian motion may affect the DRM should become

larger. Using $\alpha = MVB/\kappa T$, $\alpha < 1$, $B = 60~\mu T$ and T = 300~K, with NRM values in the range of 0.1– $10~A~m^{-1}$ for igneous samples with magnetic silicates gives upper sizes of ~ 2.0 – $9.4~\mu m$. This indicates that Brownian motion may influence the smallest silicate grains that host magnetic mineral inclusions.

Next we consider how post-depositional sedimentary processes affect the DRM recorded by magnetic mineral inclusions. It is difficult to assess potential effects because we did not perform controlled PDRM experiments or simulations here. Post-depositional realignment in our experiments is probably negligible even with reduced friction experienced by the particles, although some particles may have rotated after deposition. Post-depositional processes, such as bioturbation, can remobilize small magnetic particles to produce a PDRM (Kent 1973; Roberts et al. 2013) that in some cases completely erase the original DRM (Zhao et al. 2016). Postdepositional perturbations are also likely to affect DRM signals carried by magnetic inclusion-bearing silicates. Nevertheless, our experimental DRM data confirm directly that magnetic inclusion bearing silicates can record a palaeomagnetic signal, albeit subject to inclination shallowing. Given the potentially widespread occurrence of magnetic mineral inclusions within host silicates in many sedimentary environments (e.g. Hounslow & Maher 1996; Chang et al. 2016a, b; Hatfield et al. 2013, 2017), and that silicate host grains protect iron oxide inclusions and their remanence against potential post-depositional diagenesis (Roberts 2015; Chang et al. 2016b), magnetic inclusion-bearing silicates expand the range of relevant materials for sedimentary palaeomagnetic studies.

4.3 Possible cause of inclination shallowing for silicates with magnetic inclusions

Our DRM data indicate variable inclination shallowing, which could also produce a latitude dependent DRM intensity (Fig. 8), as suggested by Molinek & Bilardello (2018) who also proposed an anisotropy-based correction for such biased RPI data. Our DRM data indicate a larger degree of inclination shallowing (smaller f values; Figs 6b and d), compared to published data for many natural samples. For example, Bilardello & Kodama (2010) found that for Carboniferous red beds of western Newfoundland and a compilation of published data the inclination shallowing factor f is in the 0.54-0.79 and 0.4-0.59 ranges for magnetite-bearing and haematite-bearing samples, respectively. This is consistent with suggestions of larger inclination shallowing in laboratory deposition experiments compared to sedimentary palaeomagnetic records (e.g. Griffiths et al. 1960; Tauxe & Kent 1984; Zhao & Roberts 2010; Molinek & Bilardello 2018). Due to different depositional settings in the laboratory and natural environments, inclinations from laboratory DRM experiments may not be directly comparable to palaeomagnetic results. Previous DRM experiments on sized samples do not reveal grain size dependent inclination shallowing (e.g. Griffiths et al. 1960). DRM data from our controlled magnetic inclusion bearing silicate samples indicate a clear silicate grain size dependent inclination shallowing, where larger silicate grains have less shallowing (Figs 6b and d). SEM observations of our sized silicate samples (Fig. 2) do not reveal distinct populations of more spherical or platy particles. The silicate grain elongation is also similar among our samples, although the larger silicate sample 'gabbro $20-30 \mu m'$ appears to be slightly larger compared to sample 'gabbro 10–15 μ m'. The inclination flattening mechanism proposed by King (1955) who suggested that inclination error arises from different populations of spherical and platy particles (aligning with the field and horizontal plane, respectively) is unlikely to explain our inclination data trend (i.e. larger particles have larger elongations and, therefore, have larger degree of inclination shallowing; Figs 6b and d). Instead, the 'rolling ball' model of Griffiths et al. (1960), which has been tested by various authors (Tauxe and Kent 1984; Bilardello 2013; Bilardello et al. 2013), suggests that particles roll into the nearest depression between grains on the sedimentation plane to produce an inclination error. Smaller particles would more likely fall into the pores (therefore producing larger inclination errors than larger particles), which may explain our observed size-dependent inclination flattening. For example, rolling in random directions produces shallower inclinations by introducing a bias toward the horizontal without a declination bias. Jezek et al. (2012) simulated numerically the effect of particle rolling on inclination shallowing. Their simulations demonstrate that mixing small magnetic particles with larger non-magnetic particles would effectively increase the amount of rolling and exacerbate inclination shallowing. Larger silicate particles are assumed to be less prone to rolling than smaller grains, which could produce a smaller inclination error, as shown in our experimental DRM data (Fig. 6).

5 CONCLUSIONS

The following conclusions are reached from our laboratory deposition study. (1) Magnetic mineral inclusions hosted within silicate particles (with $10-50~\mu m$ sizes) can record a DRM with shallow inclinations, which confirms previous palaeomagnetic findings (Chen et al. 2017; Hong et al. 2019) and numerical calculations (Chang et al. 2016a). (2) The degree of inclination shallowing depends on

silicate size, where larger silicate grains have smaller inclination errors. A 'rolling ball' model might explain this size dependent inclination shallowing. (3) DRM results confirm directly that deposition of non-magnetic silicate grains with magnetic mineral inclusions is a further cause of low-efficiency of sedimentary remanence acquisition and quasi-linear field dependence in addition to flocculation (e.g. Shcherbakov & Shcherbakova 1983; Tauxe et al. 2006). (4) DRM intensity varies non-linearly with applied field for deposited silicate particles with magnetic mineral inclusions. The curvature of this relationship is likely caused by the magnetic moment distributions of embedded magnetic inclusions and by host silicate size and shape. Non-magnetic host particles with magnetic mineral inclusion assemblages appear to behave differently from unprotected magnetic particles during sediment remanence acquisition. Given the widespread occurrence of host particles with magnetic mineral inclusions in sedimentary environments, their contributions to sedimentary palaeomagnetic signals are likely to be important.

ACKNOWLEDGEMENTS

We thank Prof Bing Shen (Peking University) for suggestions on chemical dissolution of Fe-Ti oxides and for providing access to his chemistry laboratory, and Prof Chunhui Tao for providing the basalt sample. We thank Dario Bilardello and Ramon Egli for providing thorough reviews that improved the paper significantly, and Eduard Petrovsky for editorial handling. This study was supported by The National Natural Science Foundation of China (NSFC grants 41722402, 41774074). LC also acknowledges funding support from a Royal Society-Newton Advanced Fellowship (NAF\R1\201096) and from the NSFC (grant 42061130214). DH and APR acknowledge funding from the Australian Research Council (grants DP120103952 and DP200100765), GAP from a NERCIndependent Research Fellowship (NE/P017266/1), LT from the NSF-NERC program (grant EAR1827263) and from NSF (grant EAR1547263), and ARM from NERC (grant NE/S001018/1). The data underlying this article are available in the article and in its online supplementary material.

REFERENCES

- Bilardello, D. & Kodama, K.P., 2010. Rock magnetic evidence for inclination shallowing in the early Carboniferous Deer Lake Group red beds of western Newfoundland, *Geophys. J. Int.*, 181(1), 275–289.
- Bilardello, D., 2013. Understanding DRM acquisition of plates and spheres: a first comparative experimental approach, *Geophys. J. Int.*, 195(1), 148–158
- Bilardello, D., Jezek, J. & Gilder, S.A., 2013. Role of spherical particles on magnetic field recording in sediments: experimental and numerical results, *Phys. Earth Planet. Inter.*, 214, 1–13.
- Butler, R.F., 1992. *Paleomagnetism: Magnetic Domains to Geologic Terranes*, Vol. **319**, Blackwell Scientific Publications.
- Chang, L., Roberts, A.P., Heslop, D., Hayashida, A., Li, J., Zhao, X. & Huang, Q., 2016a. Widespread occurrence of silicate-hosted magnetic mineral inclusions in marine sediments and their contribution to paleomagnetic recording, *J. geophys. Res.*, 121, 8415–8431.
- Chang, L. et al. 2016b. Asian monsoon modulation of nonsteady state diagenesis in hemipelagic marine sediments offshore of Japan, Geochem. Geophys. Geosyst., 17, 4383–4398.
- Channell, J.E.T., Xuan, C. & Hodell, D.A., 2009. Stacking paleointensity and oxygen isotope data for the last 1.5 Myr (PISO-1500), *Earth planet. Sci. Lett.*, 283, 14–23.
- Chen, L. et al. 2017. Remanence acquisition efficiency in biogenic and detrital magnetite and recording of geomagnetic paleointensity, Geochem. Geophys. Geosyst., 18, 1435–1450.

- Collinson, D.W., 1965. DRM in sediments, J. geophys. Res., 70, 4663–4668.
 Egli, R., Chen, A.P., Winklhofer, M., Kodama, K.P. & Horng, C.S., 2010.
 Detection of noninteracting single domain particles using first-order reversal curve diagrams, Geochem. Geophys. Geosyst., 11, Q01Z11, doi:10.1029/2009GC002916.
- Egli, R., 2013. VARIFORC: an optimized protocol for calculating nonregular first-order reversal curve (FORC) diagrams, *Global Planet. Change*, 110, 302–320.
- Egli, R. & Zhao, X., 2015. Natural remanent magnetization acquisition in bioturbated sediment: general theory and implications for relative paleointensity reconstructions, *Geochem. Geophys. Geosyst.*, 16(4), 995–1016.
- Evans, M.E., McElhinny, M.W. & Gifford, A.C., 1968. Single domain magnetite and high coercivities in a gabbroic intrusion, *Earth planet. Sci. Lett.*, 4(2), 142–146.
- Gradstein, F.M., Ogg, J.G., Schmitz, M.D. & Ogg, G.M., 2012. The Geologic Time Scale, Elsevier, doi:10.1016/B978-0-444-59425-9.01001-5.
- Griffiths, D.H., King, R.F., Rees, A.I. & Wright, A.E., 1960. The remanent magnetism of some recent varved sediments, *Proc. R. Soc. A*, 256(1286), 359–383.
- Harrison, R.J. & Feinberg, J.M., 2008. FORCinel: an improved algorithm for calculating first-order reversal curve distributions using locally weighted regression smoothing, *Geochem. Geophys. Geosyst.*, 9(5), G05016, doi:10.1029/2008GC001987.
- Hatfield, R.G., Stoner, J.S., Carlson, A.E., Reyes, A.V. & Housen, B.A., 2013. Source as a controlling factor on the quality and interpretation of sediment magnetic records from the northern North Atlantic, *Earth planet. Sci. Lett.*, 368, 69–77.
- Hatfield, R.G., Stoner, J.S., Reilly, B.T., Tepley, F.J., III, Wheeler, B.H. & Housen, B.A., 2017. Grain size dependent magnetic discrimination of Iceland and South Greenland terrestrial sediments in the northern North Atlantic sediment record, *Earth planet. Sci. Lett.*, 474, 474–489.
- Heslop, D., Witt, A., Kleiner, T. & Fabian, K., 2006. The role of magnetostatic interactions in sediment suspensions, *Geophys. J. Int.*, 165, 775–785.
- Heslop, D., 2007. Are hydrodynamic shape effects important when modelling the formation of depositional remanent magnetization?, *Geophys. J. Int.*, 171, 1029–1035.
- Heslop, D. & Roberts, A.P., 2012. Estimation of significance levels and confidence intervals for first-order reversal curve distributions, *Geochem. Geophys. Geosyst.*, 13, Q12Z40, doi:10.1029/2012GC004115.
- Hong, H., Chang, L., Hayashida, A., Roberts, A.P., Heslop, D., Paterson, G.A., Kodama, K. & Tauxe, L., 2019. Paleomagnetic recording efficiency of sedimentary magnetic mineral inclusions: implications for relative paleointensity determinations, *J. geophys. Res.*, 124, 6267–6279.
- Hounslow, M.W. & Maher, B.A., 1996. Quantitative extraction and analysis of carriers of magnetization in sediments, Geophys. J. Int., 124, 57–74.
- Hounslow, M.W. & Morton, A.C., 2004. Evaluation of sediment provenance using magnetic mineral inclusions in clastic silicates: comparison with heavy mineral analysis, *Sediment. Geol.*, 171(1-4), 13–36.
- Jezek, J. & Gilder, S.A., 2006. Competition of magnetic and hydrodynamic forces on ellipsoidal particles under shear: influence of the Earth's magnetic field on particle alignment in viscous media, *J. Geophys. Res.*, 111, B12S23, doi:10.1029/2006JB004541.
- Jezek, J., Gilder, S.A. & Bilardello, D., 2012. Numerical simulation of inclination shallowing by rolling and slipping of spherical particles, *Comput. Geosci.*, 49, 270–277.
- Johnson, E.A., Murphy, T. & Torreson, O.W., 1948. Pre-history of the Earth's magnetic field, *Terr. Magn. Atmos. Electr.*, 53, 349–372.
- Kent, D.V., 1973. Post depositional remanent magnetization in deep-sea sediments, *Nature*, 246, 32–34.
- King, R.F., 1955. The remanent magnetism of artificially deposited sediments, *Geophys. J. Int.*, 7, 115–134.
- Lascu, I., Einsle, J.F., Ball, M.R. & Harrison, R.J., 2018. The vortex state in geologic materials: a micromagnetic perspective, *J. geophys. Res.*, 123, 7285–7304.
- Levi, S. & Banerjee, S.K., 1976. On the possibility of obtaining relative paleointensities from lake sediments, *Earth planet. Sci. Lett.*, **29**, 219–226

- Maher, B.A., Watkins, S.J., Brunskill, G., Alexander, J. & Fielding, C.R., 2009. Sediment provenance in a tropical fluvial and marine context by magnetic 'fingerprinting' of transportable sand fractions, *Sedimentology*, 56(3), 841–861.
- Mitra, R. & Tauxe, L., 2009. Full vector model for magnetization in sediments, Earth planet. Sci. Lett., 286, 535–545.
- Molinek, F.R. & Bilardello, D., 2018. Application of an anisotropy-based correction to relative paleointensity estimates of experimentally deposited sediments, *Geochem. Geophys. Geosyst.*, 19, 882–900.
- Muxworthy, A., Heslop, D. & Williams, W., 2004. Influence of magnetostatic interactions on first-order-reversal-curve (FORC) diagrams: a micromagnetic approach, *Geophys. J. Int.*, 158(3), 888–897.
- Muxworthy, A.R. & Evans, M.E., 2013. Micromagnetics and magnetomineralogy of ultrafine magnetite inclusions in the Modipe Gabbro, *Geochem. Geophys. Geosyst.*, **14**, 921–928.
- Muxworthy, A.R., Evans, M.E., Scourfield, S.J. & King, J.G., 2013. Paleointensity results from the late-Archaean Modipe Gabbro of Botswana, *Geochem. Geophys. Geosyst.*, **14**, 2198–2205.
- Nagata, T., 1961. Rock Magnetism. Maruzen Company.
- Newell, A.J., 2005. A high-precision model of first-order reversal curve (FORC) functions for single-domain ferromagnets with uniaxial anisotropy, *Geochem. Geophys. Geosyst.*, **6**, Q05010, doi:10.1029/02004GC000877.
- Paterson, G.A., Wang, Y. & Pan, Y., 2013. The fidelity of paleomagnetic records carried by magnetosome chains, *Earth planet. Sci. Lett.*, 383, 82–91.
- Roberts, A.P., 2015. Magnetic mineral diagenesis, *Earth-Sci. Rev.*, **151**, 1–47.
- Roberts, A.P., Pike, C.R. & Verosub, K.L., 2000. First-order reversal curve diagrams: a new tool for characterizing the magnetic properties of natural samples, *J. geophys. Res.*, **105**, 28461–28475.
- Roberts, A.P., Tauxe, L. & Heslop, D., 2013. Magnetic paleointensity stratigraphy and high-resolution quaternary geochronology: successes and future challenges, *Quat. Sci. Rev.*, 61, 1–16.
- Roberts, A.P., Heslop, D., Zhao, X. & Pike, C.R., 2014. Understanding fine magnetic particle systems through use of first-order reversal curve diagrams, *Rev. Geophys.*, 52, 557–602.
- Roberts, A.P. et al. 2017. Resolving the origin of pseudo-single domain magnetic behavior, J. geophys. Res., 122, 9534–9558.
- Shcherbakov, V.P. & Shcherbakova, V.V., 1983. On the theory of depositional remanent magnetization in sedimentary rocks, *Geophys. Surv.*, 5, 369– 380.
- Shcherbakov, V. & Sycheva, N., 2010. On the mechanism of formation of depositional remanent magnetization, *Geochem. Geophys. Geosyst.*, **11**(2), Q02Z13, doi:10.1029/2009GC002830.
- Tao, C. et al. 2014. Seafloor hydrothermal activity and polymetallic sulfide exploration on the southwest Indian ridge, Chin. Sci. Bull., 59(19), 2266– 2276.
- Tarduno, J.A. & Cottrell, R.D., 2005. Dipole strength and variation of the time-averaged reversing and nonreversing geodynamo based on Thellier analyses of single plagioclase crystals, *J. geophys. Res.*, 110, B11101, doi:10.1029/2005JB003970.
- Tarduno, J.A., Cottrell, R.D. & Smirnov, A.V., 2001. High geomagnetic field intensity during the mid-Cretaceous from Thellier analyses of single plagioclase crystals, *Science*, 291, 1779–1783.
- Tarduno, J.A., Cottrell, R.D. & Smirnov, A.V., 2006. The paleomagnetism of single silicate crystals: recording geomagnetic field strength during mixed polarity intervals, superchrons, and inner core growth, *Rev. Geophys.*, 44, RG1002, doi:10.1029/2005RG000189.
- Tauxe, L. & Kent, D.V., 1984. Properties of a detrital remanence carried by haematite from study of modern river deposits and laboratory redeposition experiments, *Geophys. J. R. astr. Soc.*, 76(3), 543–561.
- Tauxe, L., 1993. Sedimentary records of relative paleointensity of the geomagnetic field: theory and practice, *Rev. Geophys.*, 31, 319–354.
- Tauxe, L., Steindorf, J.L. & Harris, A., 2006. Depositional remanent magnetization: toward an improved theoretical and experimental foundation, *Earth planet. Sci. Lett.*, 244, 515–529.

- Tauxe, L. & Yamazaki, T., 2015. Paleointensities, in *Treatise on Geophysics*, 2nd edn, pp. 461–509, ed. Schubert, G., Elsevier.
- Ter Maat, G.W., McEnroe, S.A., Church, N.S. & Larsen, R.B., 2019. Magnetic mineralogy and petrophysical properties of ultramafic rocks: consequences for crustal magnetism, *Geochem. Geophys. Geosyst.*, **20**, 1794–1817, doi:10.1029/2018GC008132.
- Valet, J.-P., Meynadier, L. & Guyodo, Y., 2005. Geomagnetic dipole strength and reversal rate over the past two million years, *Nature*, 435, 802–805.
- Valet, J.-P., Tanty, C. & Carlut, J., 2017. Detrital magnetization of laboratoryredeposited sediments, *Geophys. J. Int.*, 210, 34–41.
- Van Vreumingen, M.J., 1993a. The influence of salinity and flocculation upon the acquisition of remanent magnetization in some artificial sediments, *Geophys. J. Int.*, 114, 607–614.
- Van Vreumingen, M.J., 1993b. The magnetization intensity of some artificial suspensions while flocculating in a magnetic field, *Geophys. J. Int.*, 114, 601–606.

- Verosub, K.L., 1977. Depositional and postdepositional processes in the magnetization of sediments, *Rev. Geophys. Space Phys.*, **15**(2), 129–143.
- Wang, S., Chang, L., Wu, T. & Tao, C., 2020. Progressive dissolution of titanomagnetite in high-temperature hydrothermal vents dramatically reduces magnetization of Basaltic Ocean crust, *Geophys. Res. Lett.*, 47(8), e2020GL087578, doi:10.1029/2020GL087578.
- Zhao, X. & Roberts, A.P., 2010. How does Chinese loess become magnetized, *Earth planet. Sci. Lett.*, **292**, 112–122.
- Zhao, X., Egli, R., Gilder, S.A. & Müller, S., 2016. Microbially assisted recording of the Earth's magnetic field in sediment, *Nat. Commun.*, 7, doi:10.1038/ncomm510673.
- Ziegler, L.B., Constable, C.G., Johnson, C.L. & Tauxe, L., 2011.
 PADM2M: a penalized maximum likelihood model of the 0–2
 Ma paleomagnetic axial dipole moment, Geophys. J. Int., 184(3), 1069–1089.